JOURNAL OF SOLID STATE CHEMISTRY **127,** 161–168 (1996)
ARTICLE NO. 0372

Ionic Conductivity in $Na^+/Pr^{3+}-\beta''-Al_2O_3$ Crystals

Joachim Köhler and Werner Urland

Institut für Anorganische Chemie and SFB 173, Callinstrasse 9, 30167 Hannover, Germany

Received April 22, 1996; in revised form August 19, 1996; accepted August 22, 1996

DEDICATED TO PROF. DR. DR. H.C. HANS GEORG VON SCHNERING ON HIS 65TH BIRTHDAY

The conduction behaviour of Pr^{3+} ion-exchanged $Na^+-\beta''$-Al_2O_3 crystals varying in degree of exchange (ξ) has been investigated by impedance spectroscopy in the temperature range 300–1000 K. The Arrhenius plots show a curvature at about 560 K to higher activation energies explainable by the beginning of lanthanide ion motion. With growing Pr^{3+} exchange, the ionic conductivity (σ) is lowered combined with an increasing activation energy (E_a). For a given degree of exchange, σ scatters about one to two orders of magnitude and E_a within 0.15–0.2 eV. These deviations can be understood by the different crystal compositions influencing the thickness of the conduction slabs and the ionic distributions. A lower in-plane cation concentration (for a given ξ) induces widened conduction channels, resulting in an increased conductivity and reduced activation energies. © 1996 Academic Press

1. INTRODUCTION

The high ionic conductivity in $Na^+-\beta''$-alumina is related to the unusual structure providing widened slabs (so-called conduction planes) for the migrating Na^+ ions. These layers separate close-packed spinel blocks containing Al^{3+} and the structure-stabilizing Mg^{2+} ions (1, 2). Because of the high mobility an equivalent amount of Na^+ ions is exchangable by other cations (3, 4). Several cations have been doped into $Na^+-\beta''$-alumina to investigate these systems for practical applications, e.g., solid-state batteries, solid-state lasers, sensor materials. The elucidation of the ionic conduction mechanism in $Na^+-\beta''$-alumina is still of interest. Ion-exchange reactions provide helpful experiments for gaining detailed insight into this phenomenon, e.g., by blocking the mobile ions with heavier, nonmobile di- or trivalent cations (5, 6). The resulting conduction properties depend on size and charge of the incorporated ions. But only a little information was available concerning the influence of lanthanide ions on the conduction behavior of $Na^+-\beta''$-alumina (7–10).

In this article impedance spectroscopic measurements are described for $Na^+/Pr^{3+}-\beta''$-Al_2O_3 crystals with varying degree of exchange (0–99%) to investigate the influence of changing Pr^{3+} content on the ionic conduction behavior of $Na^+-\beta''$-alumina.

2. EXPERIMENTAL

$Na^+-\beta''$-alumina crystals up to $7 \times 7 \times 3$ mm were grown by flux evaporation in a Na_2O-rich flux at 1690°C (11) and cut into rectangular bars with typical dimensions of $a \times b \times c = (1.9–5) \times (0.9–3.3) \times (0.1–0.3)$ mm. Anhydrous $PrCl_3$ powder was synthesized by the ammonium chloride route (12). For the ion exchange, the crystals were immersed under an argon atmosphere in molten $PrCl_3$. Generally, the degree of exchange (ξ) can be controlled roughly by varying the exchange temperature or the exposure time (9). The crystals investigated in this work were prepared by keeping the temperature constant at 790°C and tuning the exchange time for the adjustment of ξ. After the heating period during the ion exchange procedure the doped crystals were quenched to room temperature and exposed to no further heat treatments. The crystal compositions and degrees of exchange were determined by electron probe microanalysis (Cameca CAMEBAX).

For impedance spectroscopy, the crystals were sputtered on opposite faces (*bc*) with chromium and mounted on a special sample holder (10). Within this measurement cell even very thin samples could be contacted without cracking by a soft clamping between platinum wires and a final fixing with platinum paste (Demetron, Hanau). An automated apparatus, consisting of an impedance analyzer (HP 4192A) and a temperature control system (Eurotherm 818S), was used for all measurements. Impedance spectra consisting of 200 data points in the frequency range 500 Hz to 6.5 MHz were taken at 300–1000 K. To avoid hydration effects and to remove residual organic compounds of the platinum paste, the measurements were performed under flowing nitrogen from higher to lower temperatures in steps of 30–50 K. A waiting period of 30–45 min between the regulation of temperature and the beginning of measure-

0022-4596/96 $18.00
Copyright © 1996 by Academic Press
All rights of reproduction in any form reserved.

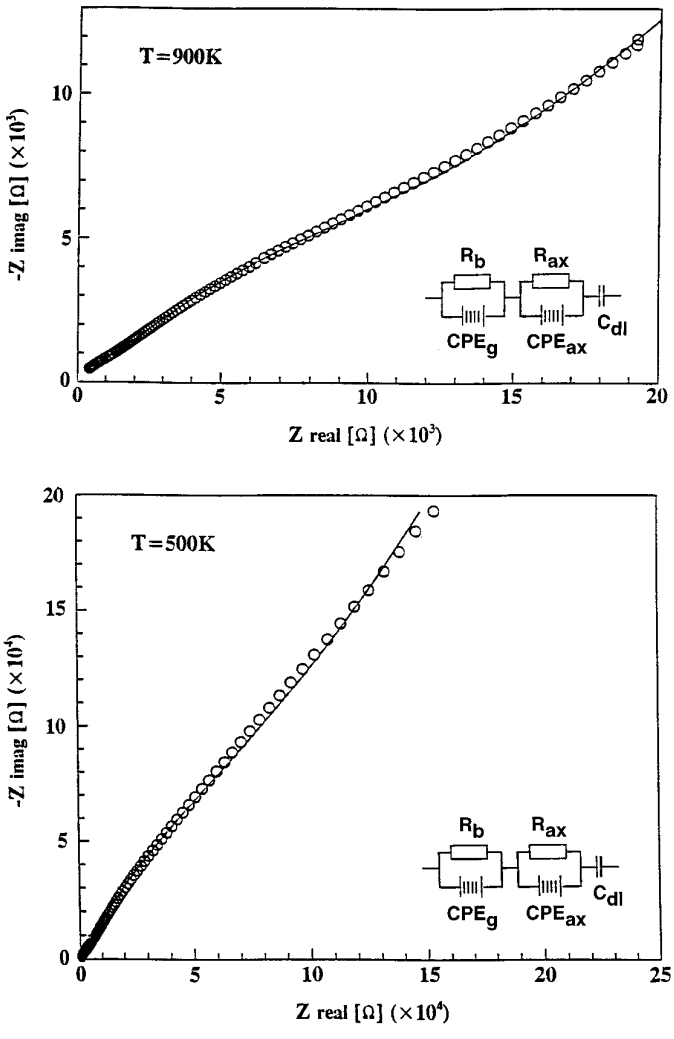

FIG. 1. Impedance spectra of $Na_{1.15}Pr_{0.13}Mg_{0.47}Al_{10.51}O_{17}$ (ξ = 25%) at 900 and 500 K, respectively: observed, ○; simulated, solid lines.

ment ensures constant temperature and homogenous distribution of the ions in the system. The specific ionic conductivities (σ) were determined from complex admittance or complex impedance plots after simulating the data with an equivalent circuit program package (13, 14).

3. RESULTS AND DISCUSSION

3.1. Impedance Spectroscopy

In Fig. 1 two representative complex impedance plots ($-Z_{imag}$ vs Z_{zeal}) of a Pr^{3+}-doped Na^+-β''-Al_2O_3 crystal with the composition $Na_{1.15}Pr_{0.13}Mg_{0.47}Al_{10.51}O_{17}$ (ξ = 25%) are given for temperatures of 900 and 500 K, respectively. The simulated curves and the applied equivalent circuit are added for comparison. The corresponding Bode plot (frequency dependence of $|Z|$ and phase angle α) at 900 K is shown in Fig. 2. The impedance spectra may be described by two overlapping, strongly depressed semicircles in the high-frequency region and an inclining straight line at lower frequencies. Impedance spectra of other Na^+/Pr^{3+}–β''-Al_2O_3 crystals, especially of the lower doped isomorphs ($\xi < 80\%$), show the same features but differ in shape as well as separation of the semicircles and straight lines depending on the degree of exchange and crystal size. As can be seen from Figs. 1 and 2, the observed frequency behavior can be simulated in good agreement by applying the equivalent circuit given in Fig. 1. In some cases the parallel constant phase elements (CPEs) are replaceable by pure capacities to give a better fit. The straight line in the impedance plots may be represented by a geometric or a double-layer capacity (index *g*, dl), whereas the deviation from 90° is caused by the roughness of the electrode surfaces (fractal geometries) (15, 16). Each of the two semicircles can be described by parallel arrangements of a resistance and a CPE or capacity. The semicircle in the high-frequency range is interpreted to result from the motion of the mobile ions within the crystal (R_b, CPE_b, b = bulk), whereas the attribution of the frequency-dependent impedance in the middle frequency region to an intrinsic bulk phenomenon is improbable because of the high resistance nature. The resulting specific conductivities of the samples would be unreasonably low, even for low-exchanged Na^+/Pr^{3+}–β''-Al_2O_3 ($\xi < 20\%$), where a decrease in σ by four to five orders of magnitude is not expected. These conductivities are not comparable to the conductivity data of other related trivalent Na^+/Ln^{3+}–β''-Al_2O_3 systems [e.g., Ln = Gd (7), Ho (10)]. Furthermore, the explanation by a second intrinsic relaxation process, e.g., by the motion of Pr^{3+} ions, is not feasible because of the apparent presence of this high-resistance impedance structure in the low temperature range ($T < 564$ K), where significant lanthanide ion mobility is not expected, and because of the ξ-independent frequency behavior. The interpretation of the second semicircle by extrinsic effects independent of the bulk properties seems more reasonable. For example, in impedance investigations of polycrystalline Na^+–β''-Al_2O_3 an additional parallel RC arrangement was introduced in the equivalent circuit for consideration of extrinsic grain boundary effects (17).

Similar phenomena in the crystals investigated for this article may be given by internal dislocations between the conduction planes due to the real mosaic crystal structure. Partial formation and intergrowth of β- and β''-alumina phases (18, 19), as well as faults of stacking sequences (planar [00.1] disorder) (20), result in blocking defects by interrupting the conduction planes with broader or displaced spinel block layers (21). Electrode effects represent a further reason influencing the impedance behavior. The dispersive structure in the middle frequency region is sensitive to modifications of experimental parameters (e.g., crys-

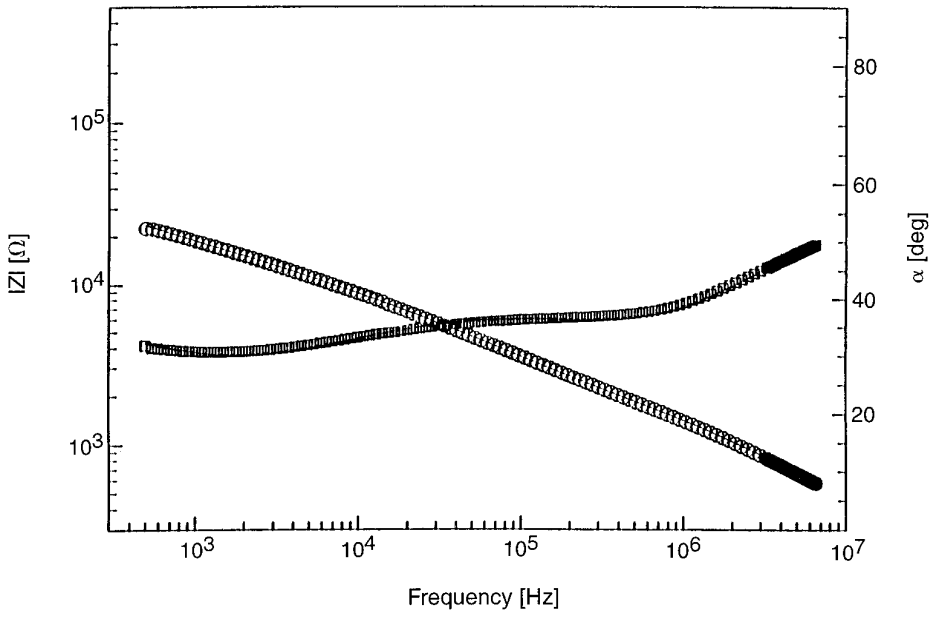

FIG. 2. Frequency dependence of $|Z|$, ○, and the phase angle α, □, of $Na_{1.15}Pr_{0.13}Mg_{0.47}Al_{10.51}O_{17}$ (ξ = 25%) at 900 K. The corresponding fits are given by the solid lines.

tal size, electrode contacting). For example, a more pronounced semicircle at middle frequencies can be achieved by splitting a parent crystal perpendicular to the crystal *c* axis, leading to increased resistance by the reduction of the electrode areas, whereas the specific resistance of the semicircle in the high-frequency region remains unaffected by this procedure. The surprisingly high resistances may be caused by the blocking effects of the platinum–chromium interface or by loose contacts between the Pt wire and the unpolished electrode areas of the crystal. Nevertheless, the second semicircle generated at lower frequencies is interpreted for further discussions to result generally from extrinsic effects (R_{ex}, CPE_{ex}, ex = extrinsic). In comparison to R_b the temperature dependence is less evident for R_{ex}. Referring to the given impedance spectra (Fig. 1), R_{ex} varies by about two orders of magnitude, whereas the changes in R_b cover three to four orders of magnitude in the measured temperature range (300–1000 K). This difference increases with growing sample resistance (in crystals with increasing ξ).

For highly exchanged Na^+/Pr^{3+}–β''-Al_2O_3 crystals ($\xi >$ 85–90%) only one very large semicircle is found in the high-frequency region of the impedance spectra, which covers the aforementioned frequency-dependent structures, and is interpreted as a dominant high bulk resistance. In these cases R_b had to be deduced graphically.

3.2. Ionic Conductivity

After R_b was determined (R_{ex} was not taken into account for further discussions) the specific bulk conductivities were calculated considering the crystal dimensions and presented in Arrhenius diagrams. In Fig. 3 a typical Arrhenius plot of some selected Na^+/Pr^{3+}–β''-Al_2O_3 crystals with different degrees of exchange is shown for comparison. Crystal compositions, conductivity data (σ) for different temperatures, activation energies (E_a) corresponding to Fig. 3 are given in Table 1. The Arrhenius curve of the

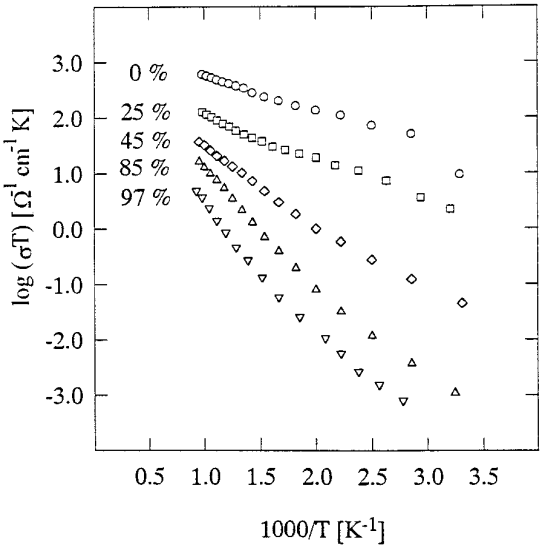

FIG. 3. Arrhenius plots of Na^+–β''-Al_2O_3 and Na^+/Pr^{3+}-β''-Al_2O_3 crystals with different degrees of exchange. The corresponding crystal compositions are given in Table 1.

TABLE 1

Crystal Composition, Degree of Exchange ξ (%), Activation Energies in the Lower (E_{a1}) and Upper (E_{a2}) Temperature Regions (eV), and Specific Ionic Conductivities σ (Ω^{-1} cm^{-1}) of Na^+–β''-Al_2O_3 and Na^+/Pr^{3+}–β''-Al_2O_3 Crystals for Some Selected Temperatures[a]

Crystal composition	ξ	E_{a1}	E_{a2}	$\sigma_{370\,K}$	$\sigma_{570\,K}$	$\sigma_{770\,K}$	$\sigma_{970\,K}$
$Na_{1.62}Mg_{0.71}Al_{10.39}O_{17}$	0	0.306	0.121	2.4×10^{-1}	3.5×10^{-1}	4.8×10^{-1}	5.6×10^{-1}
$Na_{1.15}Pr_{0.13}Mg_{0.47}Al_{10.51}O_{17}$	25	0.173	0.210	1.7×10^{-2}	7.1×10^{-2}	7.6×10^{-2}	1.2×10^{-1}
$Na_{0.88}Pr_{0.24}Mg_{0.70}Al_{10.33}O_{17}$	45	0.204	0.301	5.3×10^{-4}	3.1×10^{-3}	1.5×10^{-2}	3.0×10^{-2}
$Na_{0.24}Pr_{0.46}Mg_{0.50}Al_{10.46}O_{17}$	85	0.283	0.449	1.9×10^{-5}	2.7×10^{-4}	5.2×10^{-3}	1.6×10^{-2}
$Na_{0.04}Pr_{0.46}Mg_{0.79}Al_{10.33}O_{17}$	97	0.286	0.504	3.5×10^{-6}	5.1×10^{-5}	6.8×10^{-4}	2.6×10^{-3}

[a] Cf. Fig. 3.

undoped Na^+–β''-Al_2O_3 crystal ($\xi = 0\%$) with the composition $Na_{1.62}Mg_{0.71}Al_{10.39}O_{17}$ is determined to be analogous to the exchanged samples. The ionic conductivities and the activation energies are comparable to literature data for Na^+–β''-Al_2O_3 crystals having the composition $Na_{1.67}Mg_{0.67}Al_{10.33}O_{17}$. For these crystals E_a values of 0.264 to 0.333 eV (at temperatures below 450 K) and E_a values of about 0.10 eV for temperatures above 550 K are given (22). On the other hand, the order–disorder effect of the Na^+ ions, which is known to cause a decrease in activation energy with increasing temperature, occurs at lower temperatures ($T \approx$ 350–380 K) in $Na_{1.62}Mg_{0.71}Al_{10.39}O_{17}$ in comparison to a transition temperature of $T \approx$ 450–550 K as found in $Na_{1.67}Mg_{0.67}Al_{10.33}O_{17}$ (22). But this transition is reported to be influenced by a large number of parameters, e.g., crystal growth conditions, Mg^{2+} distribution in the spinel blocks, and Na^+ content in the planes (22). In this case, the Mg^{2+} content seems to be the dominating factor because of the apparent difference in the crystal compositions.

From Fig. 3 and Table 1 it can be seen that ionic conductivity decreases rapidly with increasing Pr^{3+} content. This is due mainly to the drastic reduction in the mobile ion concentration after an equivalent ion exchange (1 $Pr^{3+} \triangleq 3\ Na^+$). Furthermore, at low temperatures the heavier lanthanide ions block the pathways of the mobile Na^+ ions, leading to a decrease in σ, too. In comparison to divalent β''-aluminas the ionic conductivity is lowered by one to two orders of magnitude due to stronger Coulombic interactions of the trivalent lanthanide ions with the host lattice (e.g., $\sigma_{570K} = 3{,}9 \times 10^{-3}\ \Omega^{-1}\ cm^{-1}$ in Ca^{2+}–β''-Al_2O_3 (23) [see also (24, 25)]. On the other hand, σ is comparable to the conductivity data of other trivalent β''-aluminas [e.g., $\sigma_{570K} = 8 \times 10^{-5}\ \Omega^{-1}\ cm^{-1}$ in Gd^{3+}–β''-Al_2O_3 (7); see also (10)]. The observed non-Arrhenius behavior of all crystals agrees with the curvature of ionic conductivity in other Na^+/Ln^{3+}–β''-alumina systems [Ln = La (26), Gd (7), Ho (10)] and indicates a temperature-dependent number of charge carriers. Two temperature regions are defined for each crystal where the data points give a linear fit. At lower temperatures no significant Pr^{3+} ion mobility is expected and the ionic conductivity is only referred to the motion of Na^+ ions, whereas in the higher temperature range the Pr^{3+} ions are thermally activated and also become mobile, leading to an increase in σ. Stronger interactions of lanthanide ions with the spinel block anions result in the increased activation energy observable at higher temperatures. The temperature range that can be related to an increase in Pr^{3+} mobility is deduced from Arrhenius plots of all investigated Na^+/Pr^{3+}–β''-Al_2O_3 crystals to 564 ± 40 K. Thus, in the high temperature region all cations within the conduction planes contribute to the ionic conductivity, as can be stated by Fig. 4 showing the conductivity data (log σ) of all investigated crystals in dependence on ξ for two selected temperatures. A decrease in σ is observed with growing degree of exchange for temperatures below 564 ± 40 K (e.g. 374 K in Fig. 4a) due to the diminishing number of Na^+ ions, the only charge carriers in this temperature region. Above 564 ± 40 K, the additional conductivity contributions of the growing mobile Pr^{3+} ions lead to a nearly constant σ in lower-exchanged Na^+/Pr^{3+}-β''-alumina crystals ($10\% < \xi < 50\%$). The decrease in σ resulting from the loss of monovalent Na^+ ions is nearly compensated by the increased charge transport of the trivalent cations. In samples with $\xi > 50\%$ the reduction in the charge carrier concentration becomes the dominating factor again, leading to a drastically lessened conductivity. Similar correlations of the conductivity and the degree of exchange are reported in the Na^+/Sr^{2+}–β''-Al_2O_3 (27, 28), Na^+/Ba^{2+}–β''-Al_2O_3 (29), and Na^+/Pb^{2+}–β''-Al_2O_3 (30) systems for lower-exchanged crystals ($\xi < 60\%$). But interestingly, the conductivity increases again after passing a minimum at $\xi = 80\%$ in higher-doped samples of Na^+/M^{2+}–β''-Al_2O_3 (M = Ba, Pb). This minimum is interpreted to result from hydration effects (30) or from ordering phenomena within the planes which were calculated from molecular dynamics simulations to become maximal at compositions corresponding to one mobile ion per formula unit ($\xi = 80\%$) in Na^+–β''-Al_2O_3 ($Na_{1.67}Mg_{0.67}Al_{10.33}O_{17}$) (31). These orderings seems to depend on the ionic distributions

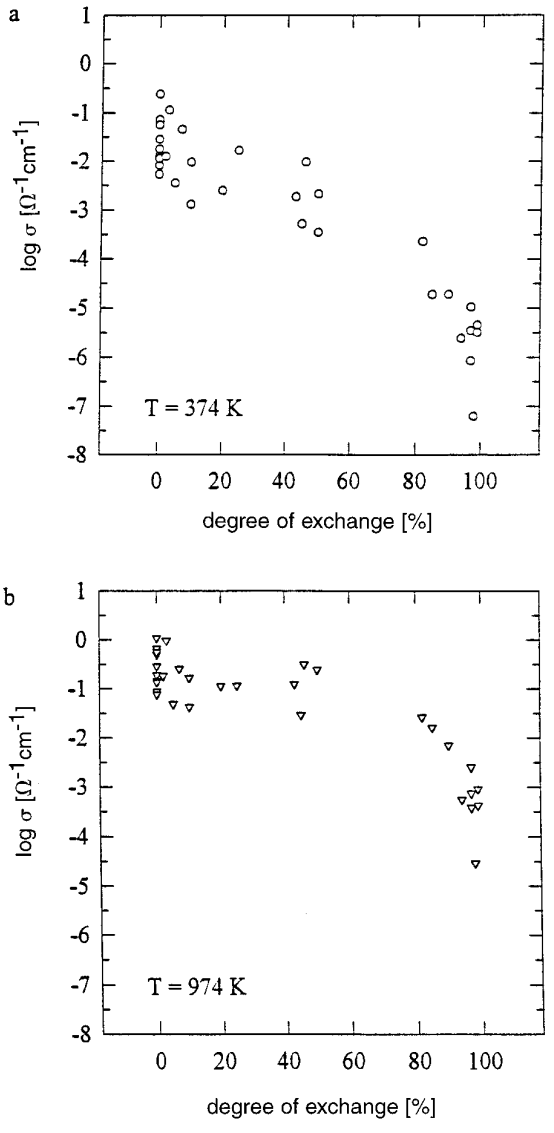

FIG. 4. Ionic conductivities (log σ) of all investigated Na^+–β''-Al_2O_3 and Na^+/Pr^{3+}–β''-Al_2O_3 crystals as a function of the degree of exchange ξ at 374 K (a) and 974 K (b).

and have been found only for Na^+/M^{2+}–β''-Al_2O_3 in which the M^{2+} ions occupy only the BR site [e.g., Ba^{2+} (29)]. In Na^+/Sr^{2+}–β''-Al_2O_3, on the other hand, the Sr^{2+} ions occupy predominantly mO positions and a continuous decrease in σ is found over the entire range of ξ (27, 28). Nevertheless, the interpretation of the conductivity data by ion–ion or by ion–vacancy correlations does not hold for the Na^+/Pr^{3+}–β''-Al_2O_3 crystals investigated in this work. Such correlations should be detectable in X-ray diffraction measurements by additional superstructure reflections. But no corresponding signals could be observed in the X-ray investigations performed on several Na^+/Pr^{3+}–β''-Al_2O_3 crystals with varying degree of exchange (26). Furthermore, the literature data are based only on cation-rich crystals corresponding to the original Na^+–β''-alumina composition of $Na_{1.67}Mg_{0.67}Al_{10.33}O_{17}$. Thus, the conduction behavior of the mixed β''-alumina systems was discussed only in terms of ξ and not with reference to the possible different crystal compositions for a given degree of exchange.

Figure 5 displays the correlation of the activation energies in the lower (E_{a1}) and the higher (E_{a2}) temperature regions with the degree of exchange for all crystals. It can be seen that E_{a2} and E_{a1} in crystals with $\xi > 30\%$ increase

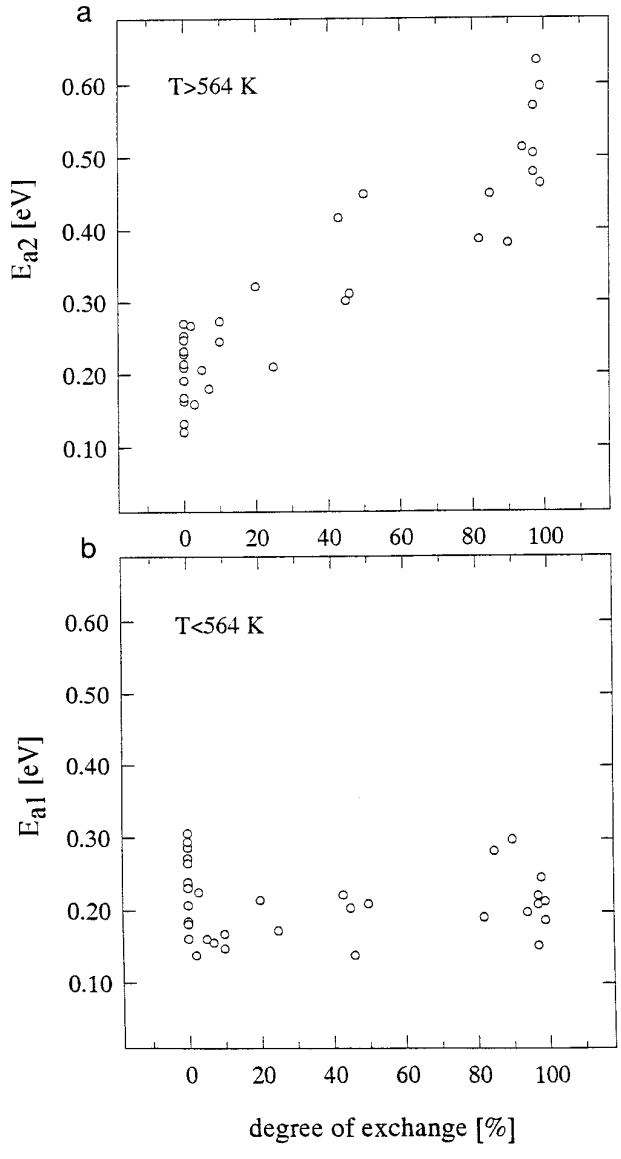

FIG. 5. Activation energies (a) E_{a2} in the upper ($T > 564$ K) and (b) E_{a1} in the lower ($T < 564$ K) temperature regions of all investigated Na^+–β''-Al_2O_3 and Na^+/Pr^{3+}–β''-Al_2O_3 crystals as a function of the degree of exchange (ξ).

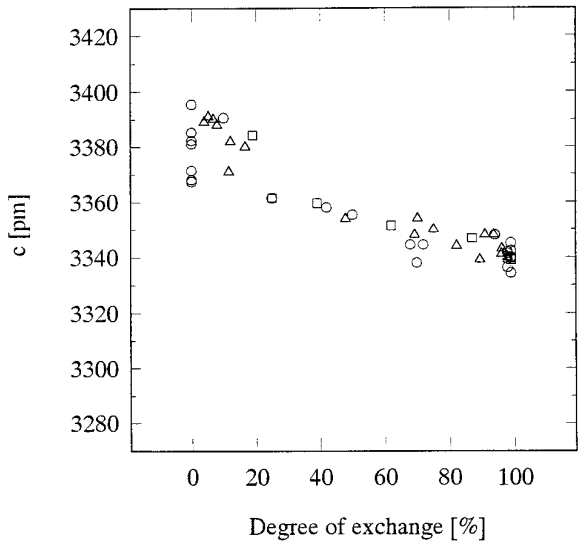

FIG. 6. Lattice parameter c (pm) as a function of the degree of exchange. Corresponding literature data are added for comparison: △, (34); □, (35).

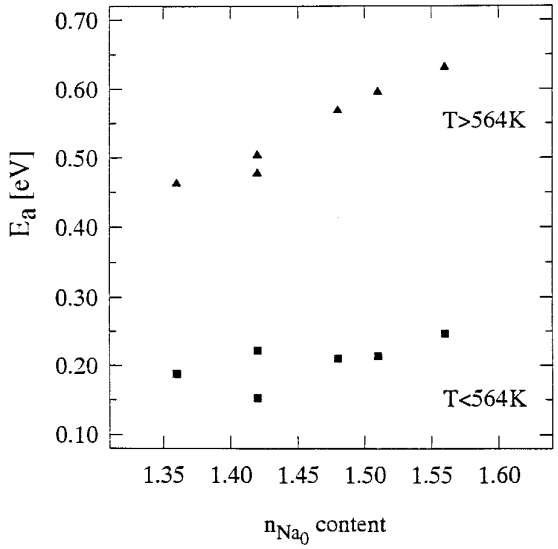

FIG. 7. Activation energies in the upper (E_{a2}, ▲) and lower (E_{a1}, ■) temperature regions as a function of the original Na^+ content per formula unit (n_{Na_0}).

continuously with growing ξ. X-ray studies on Na^+/Ln^{3+}–β''-aluminas indicate a decreasing crystallographic cell parameter c with increasing ξ [Ln = Pr, Ho (32), Er (33)] combined with shrinkage of the conduction slabs. The corresponding correlation for Na^+/Pr^{3+}–β''-Al_2O_3 crystals is displayed in Fig. 6. Thus, the cations within the planes experience a more steric restriction in mobility in the narrowed layers of higher-exchanged crystals, leading to lowered conductivities and increased activation energies. The decrease in E_{a1} for crystals with $0\% < \xi < 30\%$ results from the high activation energy at low temperatures of undoped Na^+–β''-alumina due to ordering phenomena of the Na^+ ions in the planes which have to be overcome for ionic conduction (2, 22). These arrangements are disintegrated by reducing the Na^+ ion content during the ion exchange, resulting in smaller potential barriers for the ion hopping process. In polycrystalline Na^+/Sr^{2+}–β''-Al_2O_3 the activation energies are also found to increase with growing Sr^{2+} content (27, 28).

A remarkable feature of Figs. 4 and 5 is the high scattering of σ and E_a, respectively, for a given degree of exchange. The ionic conductivity scatters about one to two orders of magnitude and E_a within 0.15–0.2 eV. An interpretation of this effect, disregarding experimental errors, is possible considering the crystal compositions. Figure 7 displays the activation energies of highly exchanged Na^+/Pr^{3+}–β''-Al_2O_3 crystals ($\xi \geq 97\%$) in the upper ($T > 560$ K) and lower ($T < 560$ K) temperature regions as a function of cation content in the conduction planes. For better elucidation E_a is plotted versus the original Na^+ content of the employed undoped Na^+–β''-alumina crystals (n_{Na_0}). n_{Na_0} is calculated from the analytically found compositions of the exchanged crystals by adding up the Na^+ and triple the Pr^{3+} content ($n_{Na_0} = n_{Na^+} + 3n_{Pr^{3+}}$) per formula unit. The corresponding data of Fig. 7 are listed in Table 2. From Fig. 7 it can be seen that a growing n_{Na_0} content causes an increased activation energy explainable again by the thickness of the conduction slabs. A high cation content within the planes leads to an attraction of the spinel blocks. This results in contracted slabs (36) and increased activation energies E_a. On the other hand, a small number of in-plane cations result in widened conduction channels combined with low activation energies for the ionic motion. The corresponding correlation

TABLE 2

Crystal Composition, Original Na^+ Content n_{Na_0}, Degree of Exchange ξ (%), and Activation Energies in the Lower (E_{a1}) and Upper (E_{a2}) Temperature Regions (eV) of Na^+/Pr^{3+}–β''-Al_2O_3 Crystals[a]

Crystal composition	n_{Na_0}	ξ	E_{a1}	E_{a2}
$Na_{0.01}Pr_{0.45}Mg_{0.62}Al_{10.48}O_{17}$	1.36	99	0.188	0.463
$Na_{0.04}Pr_{0.46}Mg_{0.61}Al_{10.46}O_{17}$	1.42	97	0.153	0.478
$Na_{0.04}Pr_{0.46}Mg_{0.79}Al_{10.33}O_{17}$	1.42	97	0.222	0.504
$Na_{0.04}Pr_{0.48}Mg_{0.51}Al_{10.50}O_{17}$	1.48	97	0.210	0.569
$Na_{0.01}Pr_{0.50}Mg_{0.72}Al_{10.35}O_{17}$	1.51	99	0.214	0.596
$Na_{0.03}Pr_{0.51}Mg_{0.54}Al_{10.46}O_{17}$	1.56	98	0.247	0.632

[a] Cf. Fig. 7.

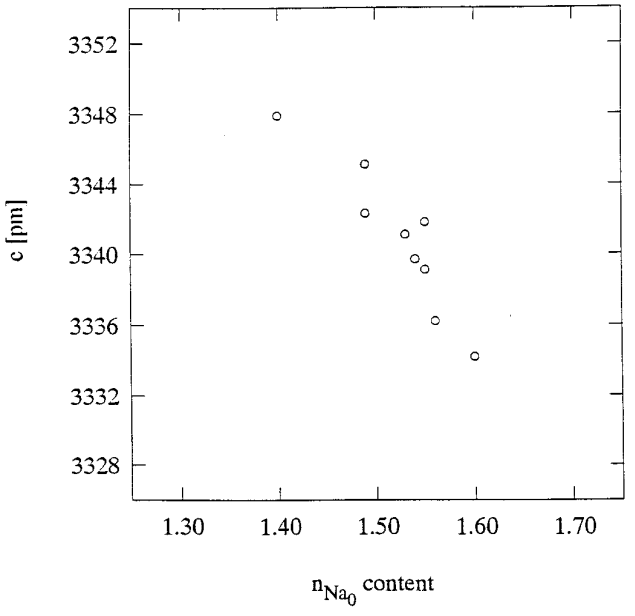

FIG. 8. Lattice parameter c (pm) of completely exchanged Na^+/Pr^{3+}–β''-Al_2O_3 crystals as a function of the original Na^+ content per formula unit (n_{Na_0}).

of the cell parameter c on the original Na^+ content n_{Na_0} is given in Fig. 8 for comparison. In the high temperature region E_{a2} is related mainly to the motion of Pr^{3+} ions, whereas E_{a1} corresponds to Na^+ mobility at lower temperatures. The Pr^{3+} ions seem to be more strongly affected by the steric restrictions because of the apparent dependence of E_{a2} on n_{Na_0} at high temperatures. On the other hand, the lower-charged Na^+ ions are more polarizable and are able to slide more easily through the narrowed passages of the shrinked conduction slabs, resulting in a lesser pronounced correlation of E_{a2} and n_{Na_0} for temperatures below 564 K.

A second fact may be important in controlling σ and E_a. X-ray studies of highly exchanged Na^+/Pr^{3+}–β''-Al_2O_3 crystals ($\xi \geq 94\%$) differing in cation content indicate a correlation between n_{Na_0} and the Beevers–Ross (BR) site occupany by Pr^{3+} ions (26, 37). The widened slabs of Na_0-poor Na^+/Pr^{3+}–β''-Al_2O_3 crystals result in a raised Pr^{3+} occupancy of BR positions, whereas in Na_0-rich samples mainly mid-oxygen (mO) site occupancy is found for the lanthanide ions, as can be stated for the latter case by structural investigations of other Ln^{3+}–β''-aluminas (Ln = Nd, Gd, Eu) (38). These different occupancy ratios for Pr^{3+} ions in two distinct crystallographic positions influence the conduction behavior and may give rise to the different slopes of the E_a–n_{Na_0} plots in Fig. 7.

Diffusion coefficients of the Na^+ ions in Na^+/Pr^{3+}–β''-alumina (D_{Na}) calculated by the Nernst equation at 574 K are given in Fig. 9 together with the corresponding data for Nd^{3+}-exchanged Na^+–β''-Al_2O_3 crystals (8). Possible slight Pr^{3+} mobilities at this temperature remain unconsidered for simplification. In the case of Nd^{3+} ion exchange, only cation-rich Na^+–β''-Al_2O_3 crystals had been used [$n_{Na_0} = 1.60$–1.70 per formula unit (FU)]. With increasing degree of exchange D_{Na} decreases. For Na^+/Pr^{3+}–β''-Al_2O_3 crystals ($\xi > 50$–60%) D_{Na} is of about one to two orders of magnitude higher than that for Nd^{3+}-doped isomorphs, whereas the opposite holds for low-exchanged samples. The steric hindrance by the contracting conduction slabs seems to be the dominant factor in crystals with $\xi > 50\%$ influencing the ionic conductivity. Despite a lower charge carrier concentration (Na^+) in the Pr^{3+}-exchanged samples D_{Na} is larger in Na^+/Pr^{3+}-β''-alumina than in the cation-rich Na^+/Nd^{3+}–β''-alumina. On the other hand, in low lanthanide ion concentrated samples ($\xi < 50\%$), D_{Na} is controlled by the Na^+ content. Although the conduction slabs are widened in the cation-poor Na^+/Pr^{3+}–β''-Al_2O_3 crystals ($n_{Na_0} < 1.60$/FU) D_{Na} is smaller compared with the corresponding values of the Nd^{3+} isomorphs (with $n_{Na_0} > 1.60$/FU). Analogous investigations on Ho^{3+} ion-exchanged Na^+–β''-aluminas confirm this dependence of D_{Na} on the thickness of the conduction slabs and the charge carrier concentration (Na^+) (10). The transition where the height of the conduction slabs becomes the determining parameter is expected for ξ = 40–50% (for Pr^{3+} exchange). For this range the crystallographic lattice parameter c of 3355–3358 pm has been deduced from X-ray

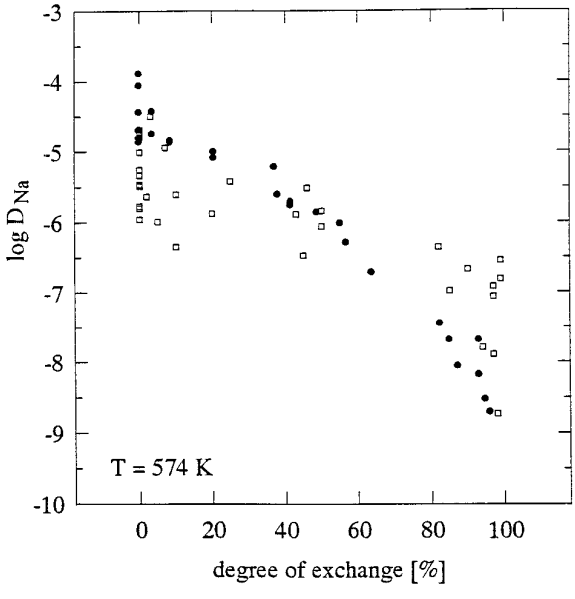

FIG. 9. Na^+ diffusion coefficients (log D_{Na}) at 574 K for Na^+/Pr^{3+}–β''-Al_2O_3 crystals, □, as a function of the degree of exchange (ξ). Corresponding data for Na^+/Nd^{3+}–β''-Al_2O_3 crystals, ●, are given for comparison (8).

studies (see Fig. 6). With this information a height of 253–254 pm can be estimated from a simple equation given in (39).

4. CONCLUSIONS

The ionic conductivity in Pr^{3+}-exchanged Na^+–β''-Al_2O_3 crystals is drastically lowered (especially for samples with $\xi > 50\%$) due to reduction of the charge carrier concentration, steric hindrance by the narrowing of the conduction slabs, and blocking of the conduction pathways by the heavy lanthanide ions. It is shown that the crystal composition influences all of the three causing factors. So, care must be taken in the interpretation of conduction data for lanthanide ion-exchanged β''-aluminas because of the broad stoichiometric range for these materials.

ACKNOWLEDGMENTS

We thank Dr. J. Koepke for the analytical measurements and the Deutsche Forschungsgemeinschaft for financial support.

REFERENCES

1. M. Bettman and C. R. Peters, *J. Phys. Chem.* **73,** 1774 (1969).
2. G. C. Farrington and J. L. Briant, *in* "Fast Ion Transport in Solids" (P. Vashista, J. N. Mundy, and G. K. Shenoy, Eds.), p. 395. Elsevier/North-Holland, Amsterdam, 1979.
3. B. Dunn and G. C. Farrington, *Solid State Ionics* **9/10,** 223 (1983).
4. S. Sattar, B. Ghosal, M. L. Underwood, H. Mertwoy, M. A. Saltzberg, W. S. Frydrych, G. S. Rohrer, and G. C. Farrington, *J. Solid State Chem.* **65,** 231 (1986).
5. G. C. Farrington and B. Dunn, *Solid State Ionics* **7,** 267 (1982).
6. B. Dunn and G. C. Farrington, *Solid State Ionics* **18/19,** 31 (1986).
7. G. C. Farrington, B. Dunn, and J. O. Thomas, *Appl. Phys. A* **32,** 159 (1983).
8. B. Dunn, G. C. Farrington, and J. O. Thomas, *MRS Bull.* **14,** 22 (1989).
9. F. Tietz and W. Urland, *J. Alloys Comp.* **192,** 78 (1993).
10. F. Tietz and W. Urland, *Solid State Ionics* **78,** 35 (1995).
11. F. Tietz, J. Koepke, and W. Urland, *J. Cryst. Growth* **118,** 314 (1992).
12. G. Meyer, *Inorg. Synth.* **25,** 146 (1989).
13. B. A. Boukamp, *Solid State Ionics* **18/19,** 136 (1986).
14. B. A. Boukamp, *Solid State Ionics* **20,** 31 (1986).
15. J. B. Bates, J. C. Wang, and Y. T. Chu, *Solid State Ionics* **18/19,** 1045 (1986).
16. I. D. Raistrick, *Solid State Ionics* **18/19,** 40 (1986).
17. E. Lilley and J. E. Strutt, *Phys. Status. Solidi A* **54,** 639 (1979).
18. D. J. M. Bevan, B. Hudson, and P. T. Moseley, *Mater. Res. Bull.* **9,** 1073 (1977).
19. L. C. DeJonghe, *Mater. Res. Bull.* **12,** 667 (1977).
20. L. C. DeJonghe, *J. Mater. Sci.* **12,** 497 (1977).
21. J. O. Bovin, *Nature* **273,** 136 (1978).
22. H. Engstrom, J. B. Bates, W. E. Brundage, and J. C. Wang, *Solid State Ionics* **2,** 295 (1981).
23. J. Ni, Y. T. Tsai, and D. H. Whitmore, *Solid State Ionics* **5,** 199 (1981).
24. B. Dunn and G. C. Farrington, *Mater. Res. Bull.* **15,** 1773 (1980).
25. B. Dunn, R. M. Ostrom, R. Seevers, and G. C. Farrington, *Solid State Ionics* **5,** 203 (1981).
26. J. Köhler, Ph.D. thesis, University of Hannover, 1996.
27. G. Allitsch, P. Linhardt, and M. W. Breiter, *Solid State Ionics* **31,** 8 (1989).
28. M. W. Breiter, H. Durakpasa, G. Dorner, and P. Linhardt, *Mater. Sci. Eng. B* **3,** 125 (1989).
29. C. Lane Rohrer and G. C. Farrington, *Mater. Res. Soc. Symp. Proc.* **210,** 119 (1991).
30. G. S. Rohrer and G. C. Farrington, *J. Solid State Chem.* **85,** 299 (1990).
31. A. Pechenik, D. H. Whitmore, and M. A. Ratner, *J. Chem. Phys.* **84,** 2827 (1986).
32. F. Tietz and W. Urland, *Key Eng. Mater.* **59/60,** 175 (1991).
33. M. Wolf and J. O. Thomas, *J. Mater. Chem.* **4,** 839 (1994).
34. F. Tietz, Ph.D. thesis, University of Hannover, 1992.
35. T. Dedecke, Ph.D. thesis, University of Hannover, 1995.
36. J. Köhler and W. Urland, *J. Solid State Chem.* **124,** 169 (1996).
37. J. Köhler and W. Urland, *in* "10th International Conference on Solid State Ionics, Abstracts, Singapore, 1995," p. 17; J. Köhler and W. Urland, *Solid State Ionics* (1996), in press.
38. W. Carrillo-Cabrera, J. O. Thomas, and G. C. Farrington, *Solid State Ionics* **28/30,** 317 (1988).
39. F. Harbach, *J. Mater. Sci.* **18,** 2437 (1983).